Impact of Co^{2+} substitution on structure and magnetic properties of M-type strontium ferrite with different Fe/Sr ratios

Yang Sun(孙洋), Ruoshui Liu(刘若水), Huayang Gong(宫华扬), and Baogen Shen(沈保根)

Citation: Chin. Phys. B, 2024, 33 (**10**): 107506. DOI: 10.1088/1674-1056/ad6554
Journal homepage: http://cpb.iphy.ac.cn; http://iopscience.iop.org/cpb

What follows is a list of articles you may be interested in

Phase structure evolution and its effect on magnetic and mechanical properties of B-doped Sm_2Co_{17}-type magnets with high Fe content

Yao-Wen Li(李耀文), Zhuang Liu(刘壮), Hai-Chen Wu(吴海辰), Fang Wang(王芳), Chao-Qun Zhu(竺超群), Dong-Liang Tan(谭栋梁), Yu Liu(刘宇), Yang Yang(羊杨), Ming-Xiao Zhang(张明晓), Ren-Jie Chen(陈仁杰), and A-Ru Yan(闫阿儒)

Chin. Phys. B, 2024, 33 (**9**): 097504. DOI: 10.1088/1674-1056/ad5535

Preparation and magnetic hardening of low Ti content $(Sm,Zr)(Fe,Co,Ti)_{12}$ magnets by rapid solidification non-equilibrium method

Xing-Feng Zhang(张兴凤), Li-Bin Liu(刘立斌), Yu-Qing Li(李玉卿), Dong-Tao Zhang(张东涛), Wei-Qiang Liu(刘卫强), and Ming Yue(岳明)

Chin. Phys. B, 2024, 33 (**9**): 097503. DOI: 10.1088/1674-1056/ad58c4

First-principles study of electronic and magnetic properties of Fe atoms on Cu_2N/Cu(100)

Jiale Chen(陈佳乐) and Jun Hu(胡军)

Chin. Phys. B, 2024, 33 (**8**): 087502. DOI: 10.1088/1674-1056/ad5275

Tailoring the optical and magnetic properties of La-BaM hexaferrites by Ni substitution

Hafiz T. Ali, M. Ramzan, M Imran Arshad, Nicola A. Morley, M. Hassan Abbas, Mohammad Yusuf, Atta Ur Rehman, Khalid Mahmood, Adnan Ali, Nasir Amin, and M. Ajaz-un-Nabi

Chin. Phys. B, 2022, 31 (**2**): 027502. DOI: 10.1088/1674-1056/ac1412

Magnetoelectric memory effect in the Y-type hexaferrite $BaSrZnMgFe_{12}O_{22}$

Fen Wang(王芬), Shi-Peng Shen(申世鹏), Young Sun(孙阳)

Chin. Phys. B, 2016, 25 (**8**): 087503. DOI: 10.1088/1674-1056/25/8/087503

Impact of Co^{2+} substitution on structure and magnetic properties of M-type strontium ferrite with different Fe/Sr ratios

Yang Sun(孙洋)[1,2], Ruoshui Liu(刘若水)[3], Huayang Gong(宫华扬)[2], and Baogen Shen(沈保根)[1,2,3,4,†]

[1] *School of Rare Earths, University of Science and Technology of China, Hefei* 230026, *China*
[2] *Ganjiang Innovation Academy, Chinese Academy of Sciences, Ganzhou* 341119, *China*
[3] *Ningbo Institute of Materials Technology & Engineering, Chinese Academy of Sciences, Ningbo* 315201, *China*
[4] *Beijing National Laboratory for Condensed Matter Physics, Institute of Physics, Chinese Academy of Sciences, Beijing* 100190, *China*

(Received 25 March 2024; revised manuscript received 6 July 2024; accepted manuscript online 19 July 2024)

Ion substitution has significantly improved the performance of ferrite magnets, and cobalt remains a key area of research. Studies on the mechanism of Co^{2+} in strontium ferrite, especially $SrFe_{2n-x}Co_xO_{19-\delta}$ ($n = 6.1$–5.4; $x = 0.05$–0.20) synthesized using the ceramic method, showed that Co^{2+} preferentially enters the lattice as the Fe/Sr ratio decreases. This results in a decrease in the lattice constants a and c due to oxygen vacancies and iron ion deficiency. The impact of Co substitution on morphology is minor compared to the effect of the Fe/Sr ratio. As the Fe/Sr ratio decreases and the Co content increases, the saturation magnetization decreases. The magnetic anisotropy field exhibits a nonlinear change, generally increasing with higher Fe/Sr ratios and Co content. These changes in the performance of permanent magnets are attributed to the absence of Fe^{3+} ions at the $12k + 2a$ and $2b$ sites and the substitution of Co^{2+} at the $2b$ site. This suggests that by adjusting the Fe/Sr ratio and appropriate Co substitution, the magnetic anisotropy field of M-type strontium ferrite can be effectively optimized.

Keywords: hexaferrite, Co substitution, Raman spectra, magnetic properties

PACS: 75.30.Gw, 75.47.Lx, 87.64.kp, 68.55.Ln **DOI:** 10.1088/1674-1056/ad6554

1. Introduction

M-type strontium ferrite ($SrFe_{12}O_{19}$: SrM) is widely used in various applications because of its cost-effectiveness, strong chemical stability, and superior magnetic properties.[1] With increasing demand for its performance, ion replacement techniques are still receiving considerable attention.[2,3] Specifically, La–Co substitution can simultaneously increase the saturation magnetization (M_s) and uniaxial magnetic anisotropy field (H_A) of SrM, which has been successfully commercialized for high performance.[4,5] Many studies have shown that Co^{2+} in La^{3+}–Co^{2+} co-substitution is considered to be the key reason for improving the magnetic properties.[6,7] That is why some researchers are aimed at Co occupation research to explain the origin of magnetic property changes. Fe^{3+} ions in hexagonal SrM occupy different crystalline sites: octahedral sites ($12k$, $2a$, and $4f_2$), tetrahedral site ($4f_1$), and trigonal bipyramid site ($2b$).[8] This relatively complex crystal structure has created many obstacles in the study of the associated mechanism of magnetic properties, but much progress has been made.

In recent years, many studies have been conducted on classical La^{3+}–Co^{2+} substitution, mainly because it is the unquenched orbital moments of Co that can play an important role in ferrites.[9–11] The Y^{3+}–Co^{2+},[12] Sm^{3+}–Co^{2+},[13] and Nd^{3+}–Co^{2+}[14] series of substitution studies have laid down the core role of Co^{2+}. The effect of Co ions has also been investigated in Co-substituted SrM samples prepared using various methods, such as the traditional solid-state reaction and sol–gel methods. To clarify the anisotropy of the Co^{2+} single ion, Liu *et al.*[15] successfully produced Co-substituted $SrFe_{12-x}Co_xO_{19}$ single crystals with $0 \leq x \leq 0.31$ using the Na_2CO_3 flux method. H_A was boosted by 19% when $0.03 \leq x \leq 0.11$ at 5 K, with only 7% loss of M_s.

These findings demonstrate that the substitution of Co^{2+} can significantly enhance magnetocrystalline anisotropy, suggesting an effective optimization strategy for the magnetic properties of SrM. Most studies have focused on the role of Co ions, often neglecting the connection between Co and Fe. Research indicates that the hybridization between Fe and Co ions is crucial for the enhancement of La–Co-substituted SrM.[16] Based on previous conclusions from Fe/Sr research, it was found that Fe ions are deficient at different sites, which may impact Co substitution. Therefore, the relationship between the magnetic ions Fe and Co requires further investigation. In this study, we investigated the effects of Co substitution and Fe/Sr ratio on the structural and intrinsic magnetic properties of SrM. Specifically, the relationship between Fe and Co is presented through the Fe/Sr ratio and Co substitution, exploring how Co substitution affects performance in iron-deficient formulations. The aim of this study is to provide a deeper understanding of these variables to enhance the magnetic properties of Sr hexaferrite materials.

†Corresponding author. E-mail: shenbaogen@nimte.ac.cn

2. Experimental procedure

$SrFe_{2n-x}Co_xO_{19-\delta}$ (n = 6.1–5.4; x = 0.05–0.20) samples were synthesized using the ceramic method. Initially, raw material powders of $SrCO_3$ (97%), Fe_2O_3 (99%), and Co_3O_4 (99.5%) were weighed according to stoichiometric ratios. These powders were then thoroughly mixed for 3 h in a planetary ball mill equipped with agate balls at a ratio of powder to water to balls of 1:2:12. After drying the wet powder in an oven, it was sintered at 1150 °C for 1 h to obtain $SrFe_{2n-x}Co_xO_{19-\delta}$.

The crystal structure of the sample was characterized by x-ray diffraction (XRD) using a Bruker AXS D8 Advance diffractometer with a step size of 0.02° and an angular range of 20°–80° (40 kV; 40 mA; λ = 1.54184 Å). The XRD data were refined using the Rietveld method to obtain lattice parameters and phase composition. Raman spectroscopy (Renishaw inVia Raman microscope), with a laser wavelength of 532 nm and a wavenumber range of 120–900 cm^{-1}, was used to analyze the ion occupation of the sample. Scanning electron microscopy (SEM; TESCAN CLARA) was used to characterize the size and morphology of the particles. An energy-dispersive spectrometer (EDS), which was attached to the SEM, was used to analyze the distribution and semiquantification of elements in the samples. The magnetic hysteresis loop was measured at 300 K using a superconducting quantum interference device magnetometer (SQUID-VSM; Quantum Design) under ±50000 Oe. The saturation magnetization (M_s) and magnetic anisotropy field (H_A) were calculated according to the law of approach to saturation.

3. Results and discussion

3.1. Phase and structure analysis

The phase formation and structural details of the Co-substituted SrM with different Fe/Sr ratios were obtained using XRD. Figure 1 shows the XRD patterns of $SrFe_{2n-x}Co_xO_{19-\delta}$ (n = 5.4–6.1; x = 0.05–0.20) sintered at 1150 °C. After such a quantitative examination of all $SrFe_{2n-x}Co_xO_{19-\delta}$ (x = 0.05–0.20; n = 6.1–5.4) samples at sintering temperatures, the phase formation rule of Co-SrM with different Fe/Sr ratios was obtained. The XRD data were refined using TOPAS software to analyze the structural changes and obtain the ratio of the second phases in the samples, and an R_{wp} below 15% ensured the credibility of the refinement.

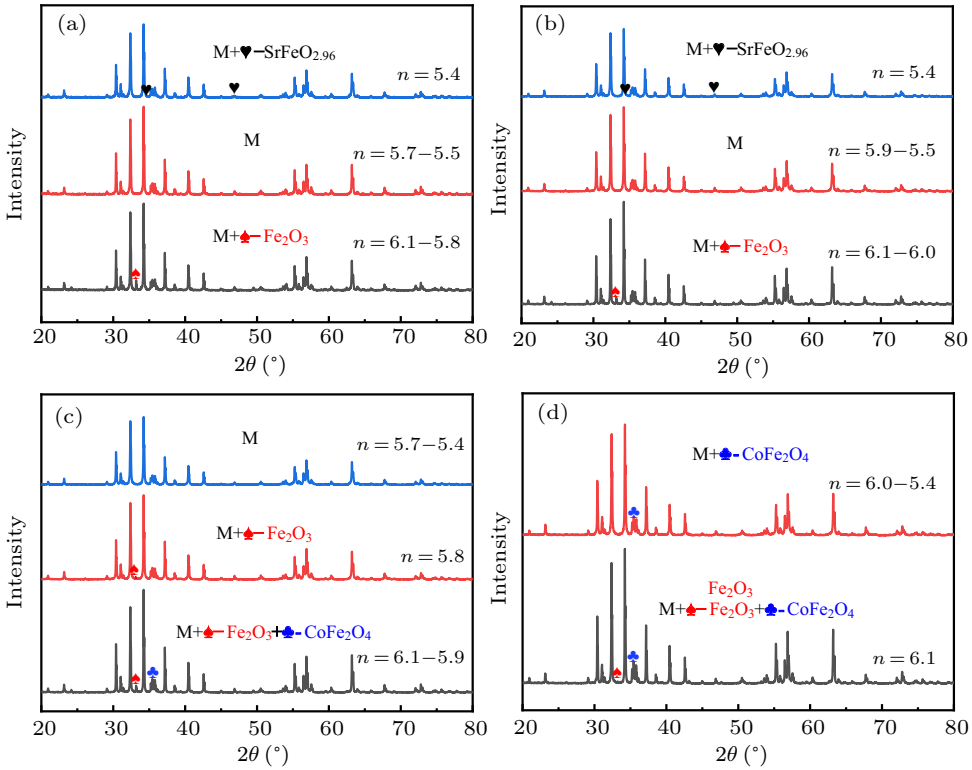

Fig. 1. XRD patterns of $SrFe_{2n-x}Co_xO_{19-\delta}$ at 1150 °C: (a) x = 0.05, (b) x = 0.10, (c) x = 0.15, and (d) x = 0.20.

A positive correlation between the increase in Fe/Sr ratio and phase-forming temperature of the samples was demonstrated. Consequently, if the Fe/Sr ratio increased, the sintering temperature of 1150 °C was not sufficient to form a pure M phase, and some of the Fe_2O_3 would remain. As can be seen in Fig. 1(a), with the values of n declining from 6.1 to 5.5, the amount of Fe_2O_3 decreased from a maximum of 4.65% to 0, and the rest was M phase remained. When $n < 5.5$,

0.96% of $SrFeO_{2.96}$ was detected in the sample because the phase formation of SrM consisted of two processes.[8] $SrCO_3$ reacted with part of the Fe_2O_3 to form an intermediate phase $SrFeO_{2.96}$, before reacting with the rest of the Fe_2O_3 to form the M phase. Therefore, the appearance of $SrFeO_{2.96}$ indicates that the amount of Fe_2O_3 was insufficient to form the M phase. As can be seen in Fig. 1(c), the Co substitution ($x = 0.15$) and Fe/Sr ratio ($n > 5.8$) continued to increase, and 4.42%–0.87% of Fe_2O_3 and 1.4%–0.87% of $CoFe_2O_4$ were detected in the samples, suggesting that as the amount of Fe_2O_3 increased, no more Fe ions could be accommodated in the lattice, and Co ions also reached the upper limit of solubility. As can be seen in Fig. 1(d), $CoFe_2O_4$ was found in the range of $n = 5.4$–5.8 when $x = 0.2$. It can be concluded that the maximum solubility of Co is 0.15 at a sintering temperature of 1150 °C.

Figure 2(a) shows the XRD refinement pattern of $SrFe_{2n-x}Co_xO_{19-\delta}$ ($n = 5.75$; $x = 0.20$) sintering at 1150 °C as an example, exhibiting a good agreement with the M-type hexagonal crystal structure (space group $P6_3/mmc$). The phase formation laws are clearly reflected in Fig. 2(b), demonstrating that the production of a single SrM phase is only possible within a specified Fe/Sr range and with a restricted Co substitution. Otherwise, there would be the production of the intermediate $SrFeO_{2.96}$ phase or $CoFe_2O_4$ formed by excess Co ions that have difficulty entering the lattice. Moreover, there are distinct effects of varying Fe/Sr ratio on the solubility of Co, with a lower Fe/Sr ratio promoting the substitution of Co.

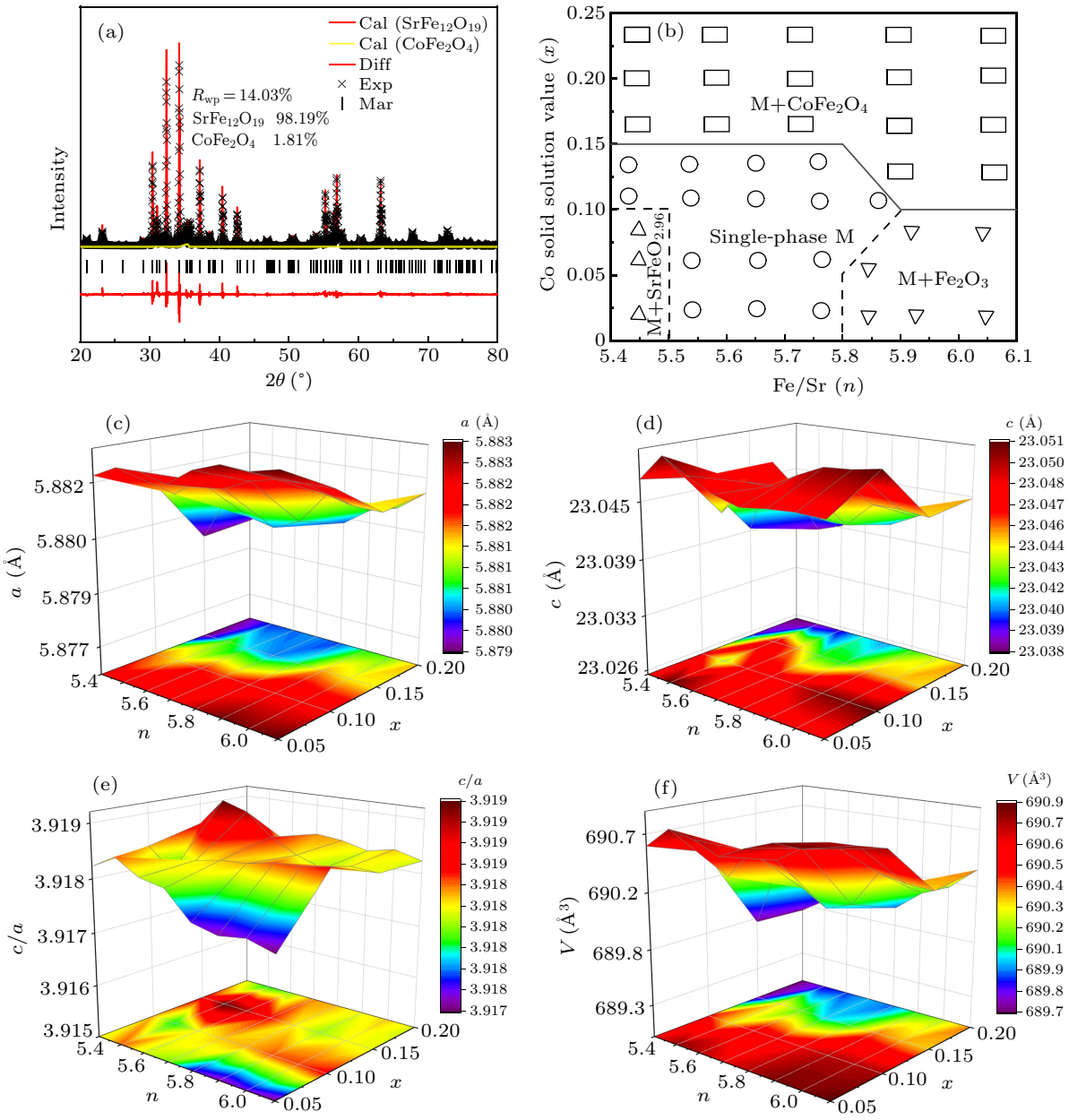

Fig. 2. (a) Refined XRD pattern of $SrFe_{11.3}Co_{0.2}O_{19-\delta}$. (b) The phase relationship between Fe/Sr and Co in $SrFe_{2n-x}Co_xO_{19-\delta}$, (c) lattice constant a, (d) lattice constant c, (e) c/a, and (f) V.

The variations in the obtained cell parameters a, c, and V are depicted in the three-dimensional contour chart shown in Figs. 2(c)–2(f), representing the variation in each parameter with the Fe/Sr ratio and Co substitution amount. In the xy plane projection, the warmth and coolness of the color indicate the level of the parameter. Figures 2(c) and 2(d) demonstrate a consistent decrease in lattice a and c when the Fe/Sr ratio decreased and Co increased. This is because the ionic diameter of Fe^{3+} (0.64 Å) was less than the radius of the Co^{2+} (0.74 Å). However, substituting Co^{2+} with Fe^{3+} causes an imbalance in the charge distribution of the system, resulting in a shortage of O^{2-} needed to maintain charge equilibrium.[15–19] Hence, the modification in a and c is a result of the interaction between the oxygen vacuum mechanism and iron ion deficiency. Figure 2(e) illustrates that the samples retained the M-type crystal structure, characterized by c/a ranging from 3.91 to 3.92. The V values were strongly influenced by changes in a (Fig. 2(f)) and decreased as the value of Co increased. Compared with the Co content, the Fe/Sr ratio had a negligible influence on the crystal structure of SrM.

3.2. Morphological analysis

The SEM images of $SrFe_{2n-x}Co_xO_{19-\delta}$ ($n = 5.9$–5.5; $x = 0.1$) sintered at 1150 °C with a single M phase are shown in Figs. 3(a)–3(e), representing the variation in grain morphology and size under different Fe/Sr ratio conditions for the same Co content. All samples showed an irregular hexagonal shape, and some small grains were not fully grown. Additionally, the size of the grains is displayed in Fig. 3(f), which was fitted using Nano Measurer software using the Gaussian equation for statistical analysis. It steadily increased as the Fe/Sr ratio decreased, in agreement with the law stated in the literature.[20] As described earlier, in the two stages of the phase formation process of the M-type hexaferrite, the intermediate phase $SrFeO_{2.96}$ was first formed and then nucleated on the surface of the remaining Fe_2O_3, which reacted with $SrFeO_{2.96}$ to form a hexagonal structure. Therefore, the Fe/Sr ratio determines the number of nuclei. Fewer nuclei lead to larger grain sizes; in contrast, more nuclei lead to grain refinement.

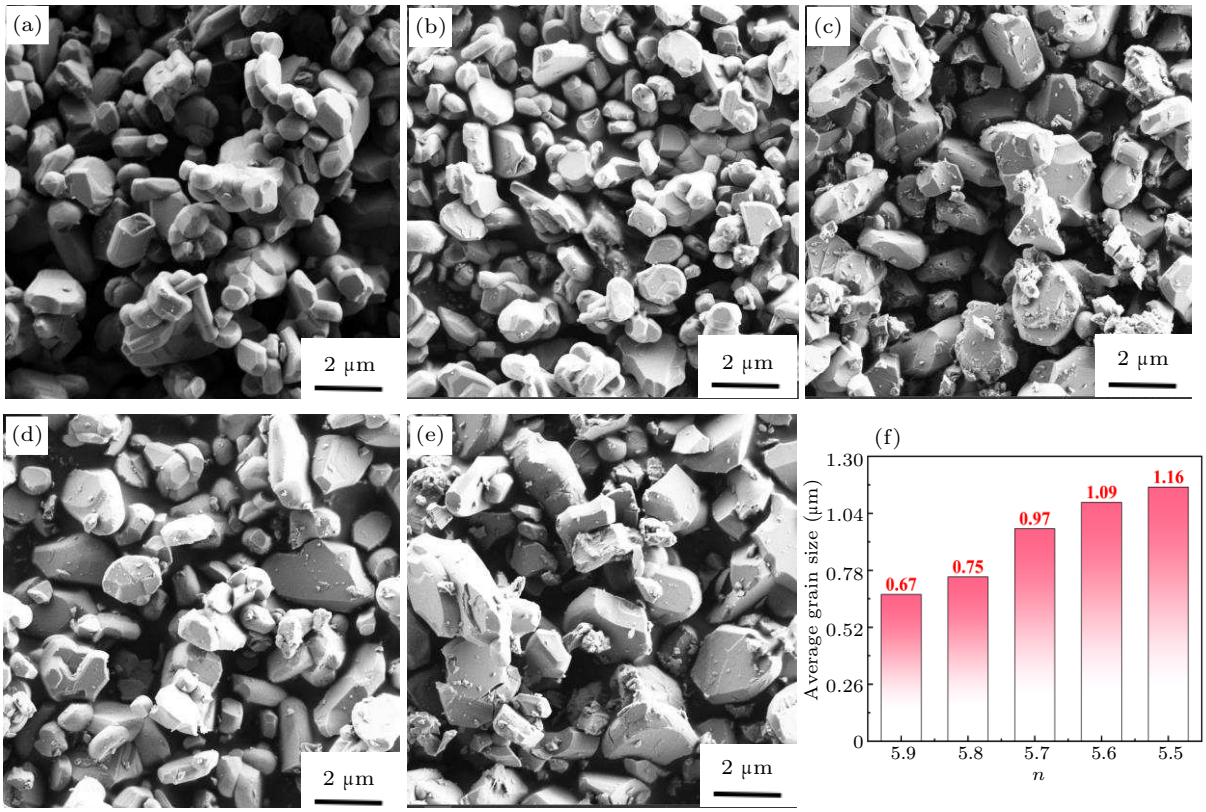

Fig. 3. SEM images and average grain size of $SrFe_{2n-0.1}Co_{0.1}O_{19-\delta}$ at 1150 °C: (a) $n = 5.9$, (b) $n = 5.8$, (c) $n = 5.7$, (d) $n = 5.6$, and (e) $n = 5.5$. (f) Average grain size.

In terms of the variation in Co substitution amount, the morphology of $SrFe_{11.5-x}Co_xO_{19-\delta}$ ($x = 0.05$–0.20) at 1150 °C is shown in Figs. 4(a)–4(d). When the Fe/Sr ratio was constant, there was no notable correlation between the grain size and Co concentration. The EDS surface scan of $SrFe_{11.5-x}Co_xO_{19-\delta}$ revealed the concentration and arrangement of Co elements, as shown in Fig. 4(e). A comparison between the theoretical Co content of the samples and the value measured by EDS showed that the actual Co content was almost identical to the expected value. A comparison of the Co element distribution maps of $SrFe_{11.35}Co_{0.15}O_{19-\delta}$ and $SrFe_{11.3}Co_{0.2}O_{19-\delta}$ revealed that the Co elements in

$SrFe_{11.3}Co_{0.2}O_{19-\delta}$ clustered together in some regions, suggesting the existence of $CoFe_2O_4$ in the sample. These results confirmed that the Co content in ferrite was close to the theoretical value, confirming the results of the phase analysis.

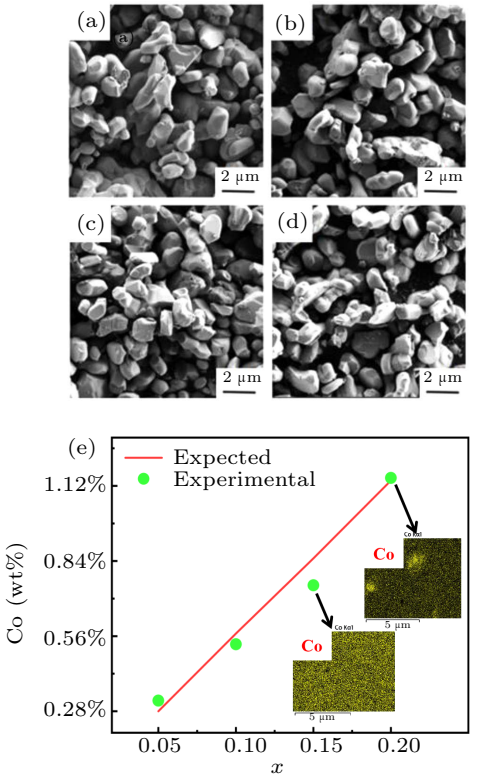

Fig. 4. SEM images of $SrFe_{11.5-x}Co_xO_{19-\delta}$ at 1150 °C: (a) $x = 0.05$, (b) $x = 0.1$, (c) $x = 0.15$, and (d) $x = 0.2$. (e) Map of the Co content and distribution.

3.3. Raman spectra

To elucidate the influence of Co^{2+} occupancy in ferrite on the magnetic characteristics, Raman spectroscopy was performed on $SrFe_{11.5-x}Co_xO_{19-\delta}$ ($x = 0.05$–0.20) and $SrFe_{2n-0.1}Co_{0.1}O_{19-\delta}$ ($n = 5.4$–6.1). Figure 5(a) shows the Raman spectra of $SrFe_{11.5-x}Co_xO_{19-\delta}$ with various Co contents between 0.05 and 0.2, which were measured at room temperature throughout the range of 120–900 cm^{-1}. Figure 5(b) shows the Raman spectra of $SrFe_{2n-0.1}Co_{0.1}O_{19-\delta}$. The displacement of Raman spectral peaks was influenced by variations in the ion mass and force constants, which were determined by factors, such as crystal structure and valence.[14,21] As the concentration of Co increased, the wave number at 684 cm^{-1} (FeO_5; $2b$ site) became broader and moved toward higher values. This change occurred as a result of the substitution of individual Co^{2+}, with Co^{2+} preferring to occupy the $2b$ site, causing a distortion in the structure. Additionally, the mass of Co^{2+} ($m_{Co} = 58.93$) was greater than that of Fe^{3+} ($m_{Fe} = 55.84$), leading to a widened peak and a shift toward higher wave numbers. Furthermore, Co^{2+} did not have any notable influence on the other sites.

In the same way, a set of samples with varying Fe/Sr of $n = 5.4$–6.1 were chosen for measurement, with a consistent Co substitution of 0.1. The Raman spectra of $SrFe_{2n-0.1}Co_{0.1}O_{19-\delta}$ exhibited changes in the peak position and widening at 337 cm^{-1} (FeO_6; $12k + 2a$ sites) and 684 cm^{-1} (FeO_5; $2b$ site). The observed variations in the Raman peaks may be attributed to the significant alteration in the occupancy rate of the $12k + 2a$ sites, as the value of n decreased from 6.1 to 5.7. This leads to a reduction in the presence of Fe^{3+} at the $12k + 2a$ sites and causes structural deformation. Furthermore, the substitution of ions also led to alterations at the $12k + 2a$ sites as a result of modifications in mass and structure caused by the set quantity of Co substitution. For Fe/Sr ranging from 5.6 to 5.4, the Raman peak at the $2b$ location exhibited a leftward shift and broadening. This suggests that there were various alterations in the iron ion vacancy sites at different Fe/Sr ratios. The other peaks exhibited negligible variations as n decreased. A relevant study showed that the presence of Fe^{3+} in the $2a$, $12k$, and $4f_1$ sublattices of SrM diminished as the value of n decreased. The order of decreasing occupancy rate was $2a > 4f_1 > 12k$. These preferences would result in varying tendencies and notable alterations in saturation magnetization.[17]

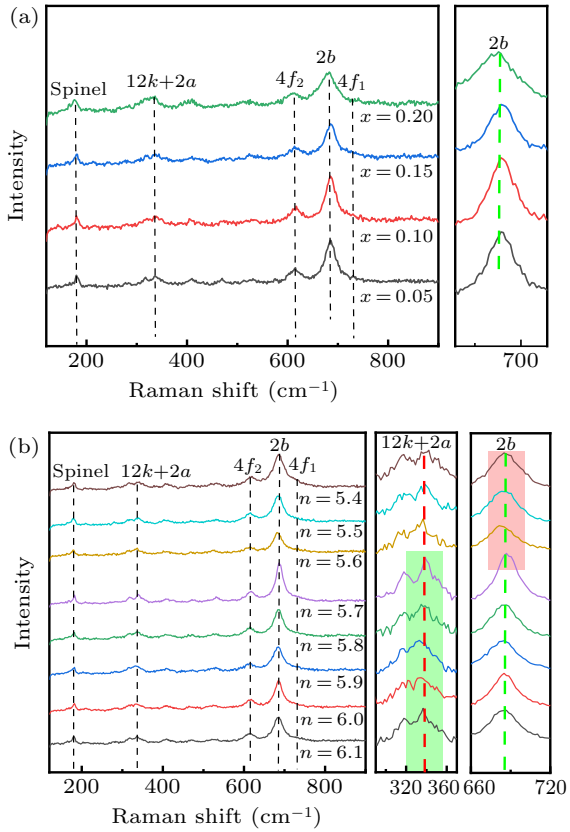

Fig. 5. (a) Raman spectra of $SrFe_{11.5-x}Co_xO_{19-\delta}$ ($x = 0$–0.20). (b) Raman spectra of $SrFe_{2n-0.1}Co_{0.1}O_{19-\delta}$ ($n = 5.4$–6.1).

3.4. Magnetic properties

The magnetic hysteresis loop of $SrFe_{2n-x}Co_xO_{19-\delta}$ ($n = 5.5$–5.9; $x = 0.10$) was measured at 300 K in the applied range of −50000 Oe to 50000 Oe (Fig. 6(a)). It can be seen that the substitution of SrM by Co at different Fe/Sr ratios affected the

magnetic properties. According to the Stoner–Wohlfarth approximation, M_s values were obtained via the law of approaching saturation (Fig. 6(b)). This can be described by Eq. (1) in the high-field region.

The Stoner–Wohlfarth (S-W) model uses the approach saturation law to predict M_s following Co substitution,[22]

$$M = M_s\left(1 - \frac{A}{H} - \frac{B}{H^2}\right) + \chi H, \tag{1}$$

where M_s is the saturation magnetization, χH is the forced magnetization induced by the field, A is a constant representing the contribution of inclusions and microstresses, and B is related to magnetocrystalline anisotropy.

As shown in Fig. 6(c), M_s improved from 69.84 emu/g to 71.90 emu/g as the Fe/Sr ratio increased from 5.5 to 5.9 with a constant Co substitution of 0.1. This suggests a positive correlation between the concentration of Fe ions in the M phase and saturation magnetization. The net magnetic moment of the molecule was determined by the vector sum of the Fe ions at different sublattices. The Fe ions were distributed in different amounts in the five nonequivalent sites, namely, 2*a*, 2*b*, and 12*k*, for upward rotation alignment, and $4f_1$ and $4f_2$ for downward rotation alignment. As shown by the results of the Raman spectra in the previous section, with a decrease in Fe/Sr ratio, Fe ions tend to be lost at the spin-up 12*k*, 2*a*, and 2*b* sites, thus leading to a decrease in M_s. Figure 6(d) illustrates the variation in M_s as Co increased within the range of $n = 5.5$–5.7. It is evident that when the concentration of Co increased at $n = 5.7$, M_s decreased from 71.51 emu/g to 69.86 emu/g. Fe^{3+} and Co^{2+} are both magnetic ions, and the electron configurations of Co^{2+} and Fe^{3+} are d^7 and d^5, respectively, according to atomic physics. Therefore, Fe^{3+} is 5 μ_B and Co^{2+} is 3 μ_B.[23] The decrease in M_s was due to the small magnetic moment of Co^{2+} occupying the 2*b* site and the decrease in Fe/Sr ratio, resulting in the loss of Fe ions at the 12*k*, 2*a*, and 2*b* sites.

Table 1 shows the values of M_s, H_c, H_A, and K_1 of $SrFe_{2n-x}Co_xO_{19-\delta}$ ($n = 5.75$, $x = 0.05$–0.20; $x = 0.10$, $n = 5.5$–5.9). When Fe/Sr = 5.75, H_c decreased from 4081 Oe ($x = 0.05$) at the beginning to 2542 Oe ($x = 0.20$) as the Co content increased. However, when Co = 0.1, with a decrease in Fe/Sr ratio, H_c decreased from 4071 Oe to 2891 Oe. It is well known that the magnitude of H_c depends on the intrinsic properties of H_A and is more externally influenced by the grain size of the sample. The SEM images illustrate how the sample particle size remained mostly unaltered because of the fixed Fe/Sr ratio and sintering temperature. Furthermore, as the Fe/Sr ratio decreased, there was a gradual increase in the particle size and a corresponding monotonic decrease in coercivity. As a result, the variation in H_c can be linked to the fluctuation in H_A. H_A and magnetic anisotropy constant (K_1) can be calculated using Eq. (2).[24,25]

The anisotropy factor B for the crystal structure of the M-type ferrite can be mathematically represented as

$$B = \frac{H_A^2}{15} = \frac{4K_1^2}{15M_s^2}. \tag{2}$$

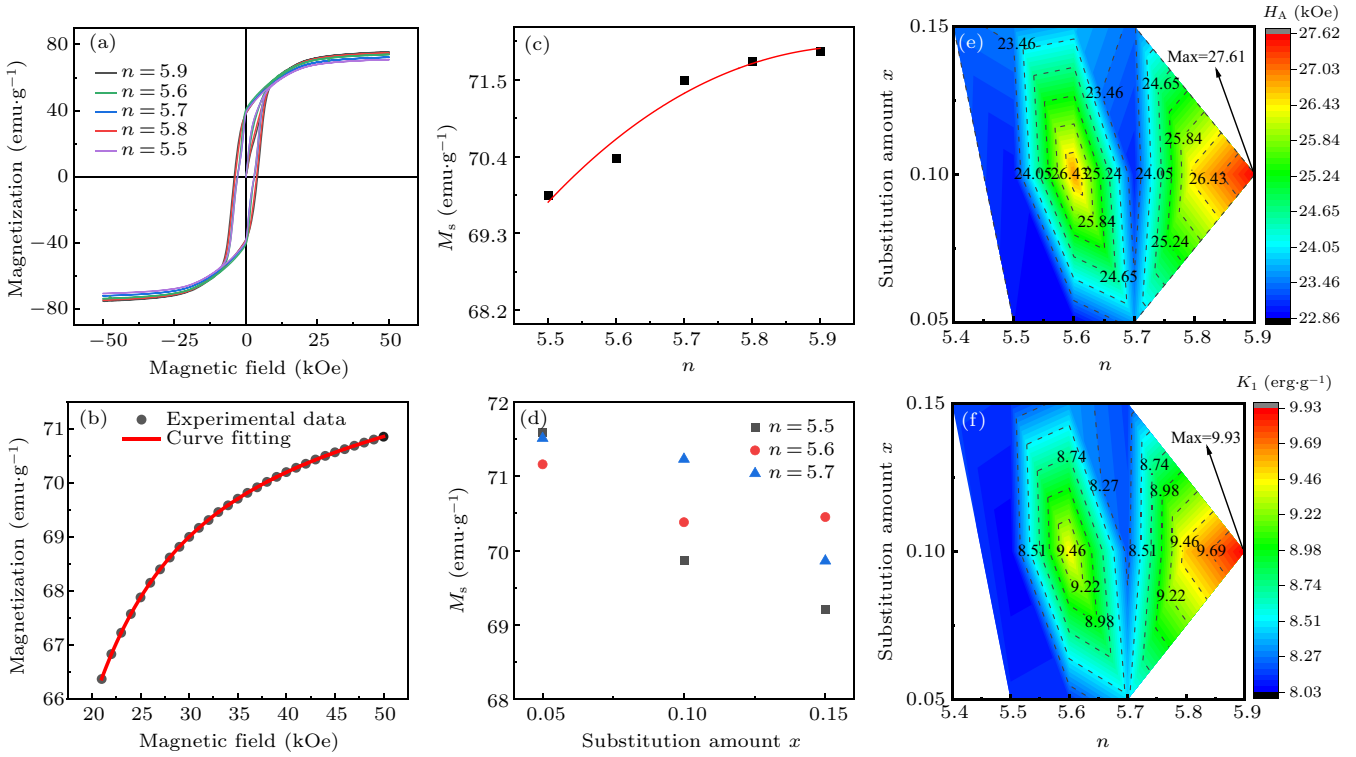

Fig. 6. (a) Hysteresis loops of $SrFe_{2n-0.1}Co_{0.1}O_{19-\delta}$ ($n = 5.5$–5.9); (b) $n = 5.7$; $x = 0.10$ using S-W to fit the example; (c) variation in M_s for $SrFe_{2n-0.1}Co_{0.1}O_{19-\delta}$ ($n = 5.5$–5.9); (d) variation in M_s for $SrFe_{2n-x}Co_xO_{19-\delta}$ ($n = 5.5$–5.7; $x = 0.05$–0.15); (e) variation in H_A for $SrFe_{2n-0.1}Co_{0.1}O_{19-\delta}$; (f) variation in K_1 for $SrFe_{2n-0.1}Co_{0.1}O_{19-\delta}$.

Notably, H_A and K_1 of $SrFe_{2n-x}Co_xO_{19-\delta}$ ($n = 5.75$; $x = 0.05$–0.20) rise initially and achieve their highest values of $H_A = 23.78$ kOe and $K_1 = 8.95 \times 10^5$ erg/g with $x = 0.10$, as seen in Table 1. To further study the effects of Co^{2+} and Fe/Sr on H_A and K_1 of SrM. The variations in H_A and K_1 of $SrFe_{2n-x}Co_xO_{19-\delta}$ ($x = 0.05$–0.20; $n = 5.4$–6.1) are depicted in the three-dimensional contour maps presented in Figs. 6(e) and 6(f). The color temperature quantified the extent of magnetic anisotropy, which exhibited nonlinear variations with both the Fe/Sr ratio and Co content when seen from different dimensions. In the *xy* plane, the central area exhibits a red region, indicating strong magnetic anisotropy. Moving toward the outer edges, the color progressively transitions to cooler tones. This indicates that when the values of x or n increase, both H_A and K_1 first increase and subsequently decrease. On the one hand, the trends in magnetic anisotropy above and below a Co substitution of 0.1 are consistent with those reported in the literature, which is mainly related to changes in the local lattice structure and Co occupancy. In the previous Raman spectra, Co ions have a high probability of occupying the 2*b* site, which contributes most to the magnetic anisotropy of M-type ferrites.[26–28] Therefore, a large substitution of a single Co will have a detrimental effect on magnetic anisotropy. On the other hand, the reason why H_A and K_1 exhibited a declining pattern when the Fe/Sr ratio decreased could be the loss of iron at the $12k + 2a$ sites. It has been reported that the 12*k* and 2*a* sites prefer planar anisotropy and are unfavorable for uniaxial anisotropy.

Table 1. Values of M_s, H_c, H_A, and K_1 for $SrFe_{2n-x}Co_xO_{19-\delta}$.

n	X	M_s (emu/g)	H_c (Oe)	H_A (kOe)	K_1 (10^5 erg/g)
5.75	0.05	73.92	4081	23.64	8.74
	0.10	71.48	3121	23.78	8.95
	0.15	71.02	3076	24.33	8.64
	0.20	69.99	2542	24.27	8.49
5.5	0.1	69.86	2891	22.99	8.03
5.6		70.38	2886	26.89	9.46
5.7		71.23	2979	23.06	8.21
5.8		71.76	3708	26.58	9.54
5.9		71.9	4071	27.61	9.93

4. Conclusions

In this study, the synthesis of $SrFe_{2n-x}Co_xO_{19-\delta}$ ($n = 6.1$–5.4; $x = 0.05$–0.20) using a ceramic method was investigated to explore the effects of Co^{2+} substitution and Fe/Sr ratio on the material structure, micromorphology, and magnetic properties. The results indicate that reducing the Fe/Sr ratio enhanced Co ion incorporation into the M phase, leading to decreased lattice parameters due to oxygen vacancies and Fe ion deficiency. The Fe/Sr ratio significantly influenced the particle growth. Raman spectroscopy revealed that Co preferably substitutes for the 2*b* site, whereas Fe ions are lost at the $12k + 2a$ sites as the Fe/Sr ratio decreases. Despite a decrease in saturation magnetization with increasing Co content, the coercivity and initial permeability peaked with minimal Co substitution, suggesting that specific Co for Fe/Sr replacement in M-type hexaferrite improved the magnetic performance.

Acknowledgements

We gratefully acknowledge the financial support from the Research Projects of Ganjiang Innovation Academy, Chinese Academy of Sciences (Grant No. E355B001), Key Research Program of the Chinese Academy of Sciences (Grant No. ZDRW-CN-2021-3), and Science Center of the National Natural Science Foundation of China (Grant No. 52088101).

References

[1] Guzmán-Mínguez J C, Fuertes V, Granados-Miralles C, Fernández J F and Quesada A 2021 *Ceram. Int.* **47** 31765
[2] Bibi F, Iqbal S, Kalsoom A, Jamshaid M, Ahmed A, Mirza M and Qureshi W A 2023 *Ceram Int.* **49** 15990
[3] Huang K, Yu J, Zhang L, Xu J, Yang Z, Liu C, Wang W and Kan X 2019 *J. Alloys Compd.* **803** 971
[4] Minachi K I 1999 *Journal of the Magnetics Society of Japan* **23** 1093
[5] Kools F, Morel A, Grossinger R, Breton J M L and Tenaud P 2002 *J. Magn. Magn. Mater.* **242–245** 12701276
[6] Pieper M W, Kools F and Morel A 2002 *Phys. Rev. B* **65** 184402
[7] Lechevallier L, Breton J M L, Teillet J, Morel A and Tenaud P 2003 *Phys. B* **327** 135
[8] Liu C, Kan X, Liu X, Feng S, Hu J, Wang W, Rehman K M U and Shezad M 2020 *Ceram. Int.* **46** 171
[9] Tyrman M, Pasko A, Barrière D L, Olivier, Mazaleyrat, Frédéric and Razek 2015 *Eur. Phys. J. Appl. Phys.* **72** 20601
[10] Huang T, Peng L, Li L, Wang R, Hu Y and Tu X 2016 *J. Rare. Earth.* **34** 148
[11] Liu R, Wang L, Xu Z, Qin C, Li Z, Yu X, Liu D, Gong H, Zhao T, Sun J, Hu F and Shen B 2022 *Mate. Today Commun.* **32** 103996
[12] Li L Z, Sokolov A, Yu C J, Li L Z, Sokolov A, Yu C J, Li Q F, Li Q F, Qian K, Vincent G and Harris 2021 *Ceram. Int.* **47** 25514
[13] Selvi K T and Priya M 2020 *J. Supercond Nov. Magn.* **33** 713
[14] Yu X, Wang L, Liu R, Zhou N, Xu Z, Gong H, Zhao T, Sun J, Hu F and Shen B 2023 *Ceram. Int.* **49** 10499
[15] Liu R, Wang L, Yu X, Xu Z, Gong H, Zhao T, Hu F and Shen B 2023 *Ceram. Int.* **49** 1888
[16] Nagasawa N, Oura M, Ikeda S, Waki T, Tabata Y, Nakamura H and Kobayashi H 2020 *J. Appl. Phys.* **128** 133901
[17] Qin C, Sun Y, Li Z, Liu R, Jing X, Wang L, Zhao T and Gong H 2023 *Arab. J. Chem.* **16** 105092
[18] Teh G B, Nagalingam S and Jefferson D A 2007 *Mater. Chem. Phys.* **101** 158
[19] Singh H K, Mohapatra P P, Dobbidi P and Chittari B L 2023 *J. Phys. D: Appl. Phys.* **56** 415304
[20] Chen D, Zeng D and Liu Z 2016 *Mater. Res. Express* **3** 045002
[21] Kreisel J, Lucazeau G and Vincent H 1998 *Int. J. Quantum Chem.* **137** 127
[22] Liu C, Kan X, Hu F, Liu X, Feng S, Hu J, Wang W, Rehman K M U, Shezad M, Zhang C, Li H, Zhou S and Wu Q 2019 *J. Alloys Compd.* **785** 452
[23] Waki T, Takao K, Tabata Y and Nakamura H 2020 *J. Solid State Chem.* **282** 121071
[24] Sharma M, Kashyap S C and Gupta H C 2014 *Phys. B* **448** 24
[25] Huang K, Yu J, Zhang L, Xu J, Yang Z, Liu C, Wang W and Kan X 2019 *J. Alloys Compd.* **803** 971
[26] Shoushtari M Z, Ghahfarokhi S E M and Ranjbar F 2012 *Advanced Materials Research* **622–623** 925
[27] Bercoff P G, Herme C and Jacobo S E 2009 *J. Magn. Magn. Mater.* **321** 2245
[28] Kreisel J, Vincent H, Tasset F, Pate M and Ganne J P 2001 *J. Magn. Magn. Mater.* **224** 17